The role of strontium in modifying aluminium-silicon alloys

M. Timpel,[1] N. Wanderka,[1] R. Schlesiger,[2] T. Yamamoto,[3] N. Lazarev,[4] D. Isheim,[5] G. Schmitz,[2] S. Matsumura,[3] and J. Banhart[1]

[1] Helmholtz-Zentrum Berlin für Materialien und Energie, Hahn-Meitner-Platz 1, 14109 Berlin, Germany

[2] Institute of Materials Physics, Westfälische Wilhelms-Universität Münster, Wilhelm-Klemm-Str. 10, 48149 Münster, Germany

[3] HVEM Laboratory, Kyushu University, Motooka 744, Nishi-ku, Fukuoka 819-0395, Japan

[4] Kharkov Institute of Physics and Technology, Akademichna St. 1, 61108 Kharkov, Ukraine

[5] Department of Materials Science and Engineering, Northwestern University, 2220 Campus Drive, Evanston, IL 60208-3108, USA

Correspondence should be addressed to: wanderka@helmholtz-berlin.de; Tel.: +49 30 8062 42079; Fax: +49 30 8062 43059

Keywords:
Eutectic modification, Al–Si-based alloys, Transmission electron microscopy, Atom probe tomography

Small amounts of strontium can transform the morphology of the eutectic silicon phase present in Al–Si casting alloys from coarse plate-like to fine fibrous networks. In order to understand this industrially important but hitherto insufficiently understood effect, the strontium distribution was studied in atomic resolution by atom probe tomography and in nanometre resolution by transmission electron microscopy. The combined investigations indicate that Sr co-segregates with Al and Si within the eutectic Si phase. Two types of segregations were found: (i) nanometre-thin rod-like co-segregations of type I are responsible for the formation of multiple twins in a Si crystal and enable its growth in different crystallographic directions; type II segregations come as more extended structures, restrict growth of a Si crystal and control its branching. We show how Sr enables both kinds of mechanisms previously postulated in the literature, namely "impurity induced twinning" (via type I) and growth restriction of eutectic Si phase (via type II).

1. INTRODUCTION

Al–Si alloys are the predominant alloys used for light metal castings due to their low weight, good castability, low cost and favourable mechanical properties. They find wide use, e.g. in automotive or aircraft applications. Solidification after casting determines the technological and mechanical properties of cast components via the resulting microstructure. One way to improve mechanical properties is to add chemical modifiers which influence microstructure formation during solidification [1]. Additions in the range of a few 100 ppm of Sr, Na, Ca, Ba or Eu modify the eutectic Si morphology from coarse plate-like into fine fibrous and have a beneficial effect on both strength and ductility [2,3]. Although the effect of chemical modification was discovered already 90 years ago [4], there is still no commonly accepted understanding of the mechanisms that allow the microstructure to change so much upon adding so little of an extra metallic ingredient. Over the past 60 years, many mechanisms of eutectic modification have been outlined in the literature, some of them concentrating on eutectic growth [3, 5–11], others on eutectic nucleation [12–15]. Overviews of predicted mechanisms of eutectic modification are given in Refs. 16–18. Two of the most established growth models of eutectic modification shall be outlined here. One of them is based on the "twin plane re-entrant edge" (TPRE) mechanism that explains the growth of the eutectic Si phase in Al–Si alloys by twinning in {111} planes [19]. This growth mechanism was first introduced for Ge and was later extended to the growth of Si crystals [10,20,21]. Accordingly, external angles between {111} planes form self-perpetuating re-entrant edges that act as favourable growth sites of the Si crystal and enable rapid growth along the <112> directions. The “restricted growth theory*”* assumes that the modifier retards Si growth by selectively adsorbing at re-entrant edges and, thus, deactivating the growth advantage of the TPRE mechanism [5,10]. Instead of growing fast as plates in few selected <112> directions, modified growth is more isotropic and covers a larger set of directions. Another widely appreciated model is "impurity induced twinning" and states that modifier atoms, e.g. Sr, are atomically adsorbed at {111} growth steps of the Si crystal. The associated change of the stacking sequence facilitates the formation of new twins and locally enables growth in many <112> directions [3]. Although these models predict different growth characteristics of the eutectic Si phase, both propose multiple twinning reactions and the formation of a high density of twins.

There is great interest in determining the inter- and intra-phase concentrations and distributions of modifiers like Sr within the eutectic microstructure. However, at typical concentrations used for eutectic modification (80-120 ppm Sr in Al–Si alloys [1]) conventional analytical methods that provide compositional information on the nm scale such as SIMS and TEM reach their resolution limit when one tries to visualise Sr distributions. Individual phase analyses by selectively dissolving Al and Si eutectic phases and subsequent atomic absorption spectroscopy indicated that the Sr modifier segregates preferentially to the eutectic Si phase during solidification but no information about the distribution of Sr within the eutectic Si phase could be given [22]. Recently, elemental mapping using X-ray fluorescence microscopy (μ-XRF) with a spatial resolution below 100 nm was used to investigate the Sr distribution in a Al–10 wt.% Si–1 wt.% Cu alloy modified by 250 ppm Sr. It was found that Sr segregates exclusively to the eutectic Si phase and the distribution of Sr within this phase is homogeneous [23]. Until now no attempts to show how the modifier is distributed within the eutectic Si phase on the atomic scale have been reported.

Recently, laser-assisted atom probe tomography (APT) has been shown to be a suitable analytical technique yielding atomic resolution [24–26] even in non-conducting materials such as Si, which is why in this work we used this technique to analyse the element distribution in Al–10 wt.% Si– 0.1 wt.% Fe alloy with additions of 200 ppm Sr in the as-cast state in order to elucidate the Sr distribution in the alloy as well as the role of Sr for the modification of the eutectic Si phase. As complementary high-resolution method, transmission electron microscopy combined with X-ray spectroscopy and high-angle annular dark-field imaging was applied to locate segregation of Sr in the alloy and to relate them to crystallographic features.

2. EXPERIMENTS

Hypoeutectic Al–10 wt.% Si alloy was cast by Rheinfelden Alloys GmbH (Rheinfelden, Germany). A mixture of about 50 kg of commercially pure Al and 5 kg of commercially pure Si were melted in an induction furnace at 760°C. The melt was degassed for 15 min using Ar and for further 5 min using Ar + Cl. For eutectic modification, an Al–10 wt.% Sr master alloy was added, after which the melt was held at 760 °C for 20 min to ensure complete dissolution. Both alloys were cast into a cylindrical permanent mould (30 mm diameter and 200 mm height) and solidified

there in about 40 s with a solidification rate in the centre of the ingot of about 8 K/s. Chemical compositions of both the unmodified and the Sr-modified Al–10Si alloy were determined using an optical emission spectrometer and are listed in Table 1. The casting rods were sectioned perpendicular to their axes. All specimens investigated in the present study were extracted at about 15–20 mm from the lower end of the ingot. For optical microscopy analysis samples were ground and polished using standard metallographic procedures. The analysis of the eutectic microstructure on the nm-scale was performed in the centres of the samples in areas displaying a well-modified eutectic structure.

For APT analysis, needle-shaped specimens of the investigated alloy with radii below 50 nm were prepared by focused ion beam (FIB) milling [27–29]. The APT used was built at the University of Münster [30]. Evaporation of atoms from the apex of the needle was performed using applied voltage superimposed by femtosecond UV laser pulses of 343 nm wavelength. A pulse energy of 150 nJ was applied for measurements of the eutectic Si phase only. 300 nJ were applied for samples with a eutectic Al/Si interface at the apex of the needle. The repetition rate was 200 kHz in both cases. Ultra-high vacuum (10^{-8} Pa) and a tip temperature of 55 K were chosen. Proxigram concentration profile analysis was performed with CAMECA's IVAS3.6 software package.

Microstructure analyses of the Sr-modified alloy were carried out using a C_s-corrected JEOL JEM ARM200F transmission electron microscope operated at 200 kV and equipped with a newly developed energy-dispersive X-ray spectroscopy (EDX) system based on a silicon drift detector with a sensing area of ~100 mm^2. The solid angle for X-ray counting was enlarged to 0.8 sr, thus increasing the counting efficiency to about 4.5 times the conventional set-up. Sr segregation within the eutectic Si phase was detected by high-resolution TEM, bright-field STEM, high-angle annular dark-field (HAADF) imaging as well as X-ray mapping, the latter two providing chemical information.

3. RESULTS

A typical eutectic microstructure of both unmodified and Sr-modified (200 ppm) Al – 10 wt.% Si–0.1 wt.% Fe alloy is shown in Fig. 1 for two different magnifications. The unmodified alloy in Fig. 1(a) and (b) reveals primary Al dendrites (bright in Fig. 1(a))

and a eutectic Si phase that appears as needles just in two dimensions but as coarse interconnected plates if viewed in three dimensions. In contrast, the modified alloy in Fig. 1(c) and (d) clearly shows the fine fibrous morphology of the eutectic Si phase. The three-dimensional morphology of such eutectic Si phase in similar Sr-modified Al–12 wt.% Si and Al–15 wt.% Si alloys has recently been studied by focused ion beam tomography [31,32].

3.1. Co-segregation type I

Figures 2(a) displays three-dimensional elemental maps of Sr (red dots) and Al (blue dots) atoms in the eutectic Si phase in a volume of 20 × 20 × 500 nm³, which is only a part of the entire analyzed volume. Si atoms are omitted for clarity. We observe a heterogeneous distribution of Sr within this volume in contrast to earlier published results obtained by X-ray fluorescence spectroscopy (μ-XRF) [9]. The volume extending from 0 to about 300 nm from the left shows largely homogeneously distributed Sr, whereas from 300 to 500 nm enrichments of Sr and Al are visible. The latter part was investigated in more detail and Fig. 2(b) presents the mapping of the Sr atom distribution only. In Fig. 2(c), Al atom positions (blue) are superposed over those of Sr (red). The compositional correlations between Sr and Al atoms visible here become even clearer in concentration depth profiles along the z-axis, see Fig. 2(d). It was surprising to detect Al in the eutectic Si phase because there has been no hint of Al segregation from any of the previous measurements described in the literature. The measured concentration of Al within the eutectic Si phase is much higher than that of Sr. In order to calculate more quantitatively the chemical composition of Sr in the co-segregation, concentration profiles were calculated utilising the proximity histogram (proxigram) method [33]. The region with co-segregation is captured by an iso-concentration surface drawn at a 0.6 at.% Sr concentration threshold, Fig. 2(e). The proxigram concentration profile is then calculated with respect to distance from that surface, with positive distances pointing towards the interior of the Al and Sr-rich region, see Fig. 2(f). In three dimensions, the morphology of such co-segregations is rod-like with a diameter up to 4 nm and a length up to 40 nm. A representative concentration of the co-segregation regions was obtained by averaging over the region 1.0–1.7 nm from the iso-surface. The rod-like co-segregation contains on average 2.6 at.% Sr, 11 at.% Al and 86.4 at.% Si.

The APT data set did not contain low-indexed planes in the high-resolution axis (investigated direction) of the APT and therefore no crystallographic information. To obtain such data, TEM was applied with a focus on the structural and compositional properties of the eutectic Si phase. To visualise the locations of Sr enrichment in the eutectic Si phase, different TEM imaging techniques were combined. Figure 3 shows a series of images of the same region obtained by (a) high-resolution TEM (HRTEM); (b) bright-field scanning TEM (BF STEM); (c) high-angle annular dark-field STEM and (d), (e) EDX mappings of both Sr and Al. The HRTEM image shows several {111} twin traces in the eutectic Si phase. They appear whenever the specimen is aligned with the appropriate <011> zone axis parallel to the electron beam. Two possible {111} co-zonal twin systems are seen, which form an angle of 70.5° to each other. BF STEM of the same region shows strong 1.5–2 nm large spots of dark contrast which occur at the intersections of twin traces as marked by circles. At the same locations in the HAADF STEM image the same spots appear in inverted contrast. What appears bright here corresponds to higher Z (atomic number) since the HAADF signal scales with Z^2. Finally, the EDX mapping for Sr in Fig. 3(d) shows increased Sr intensity compared to surrounding areas at the same locations where HAADF STEM detected Z contrast, thus providing direct evidence that Sr is segregated there. In Fig. 3(e), an Al mapping of the same region is shown. It is evident that Al is enriched in the same areas as Sr. Many areas with higher Al concentrations are visible, but not all of them belong to a co-segregation with Sr as found in the present work. Rod-like co-segregated regions as shown in Fig. 2 in three dimensions correspond to the spots appearing in the two-dimensional TEM images in Fig. 3 that are just projections along their length. This kind of co-segregation is defined as type I.

3.2. Co-segregation type II

An APT analysis and a series of TEM images of the eutectic interface between Si and Al are given in Fig. 4 and Fig. 5, respectively. Figures 4(a) (top view) and 4(b) (front view) show different projections of a three-dimensional atom reconstruction of a eutectic Al/Si interface in a Sr-modified sample with the interface along the analysed direction. The position of Al atoms (blue dots) and Sr atoms (red dots) are displayed in a reconstructed volume of 58 × 56 × 93 nm^3, which is part of a ~450 nm long analysed volume. In addition, iso-density surfaces representing 0.17 Sr atoms/nm^3

are displayed. Si atoms in the analysed volume are again omitted for clarity. Two rod-like Sr–Al–Si co-segregations with cross sections of 4 × 8 nm^2 extend from the eutectic Al/Si interface into the eutectic Si phase and are aligned in parallel, as seen in both projections. The proxigram concentration profile with respect to the iso-density surface was calculated and is shown in Fig. 4(c). Here, the rod-like co-segregation contains on average 1.1 at.% Sr, 2.5 at.% Al and 96.4 at.% Si, averaged over the region with 1.5–2.5 nm distance from the iso-density surface, and is on average 4.5 nm in diameter. Both co-segregated regions are located close to the eutectic Al/Si interface and are truncated by the surface of the analysed volume and therefore the total length of these co-segregations could be much larger than suggested by the data set. This kind of co-segregation is defined here as type II.

A corresponding series of TEM images of a type II co-segregation within the eutectic Si phase is shown in Fig. 5. It is also close to a eutectic Al/Si interface. The difference to Fig. 3 is that here we are not looking at one eutectic Si fibre but at an internal boundary between two eutectic Si fibre sections. The internal boundary lies along a {111} plane of the eutectic Si phase and is aligned parallel to the electron beam. The dashed line in Fig. 5(a) indicates the trace of the internal boundary as identified by BF STEM. One region of the internal boundary shown in Fig. 5(b) was investigated in analogy to Fig. 3. BF STEM in Fig. 5(b) indicates strong dark contrast at the internal boundary, whereas in the HAADF STEM image in Fig 5(c) the contrast is bright. EDX mappings of Sr and Al in Fig. 5(d) and 5(e), respectively, indicate co-segregation of both elements at the internal boundary of the eutectic Si phase. The width of the co-segregation measured close to the eutectic Al/Si interface is about 8 nm and its entire length along the boundary 220 nm. The width measured is in very good agreement with the result from APT.

4. DISCUSSION

The high twin density in modified Si fibres observed in the present study is in accordance with results of investigations published previously [3,20,21]. Whereas in the previous studies it has been suggested that Sr alone is responsible for the modified growth of the eutectic Si phase, the present investigations demonstrate that the growth of modified eutectic Si phase requires Sr–Al–Si co-segregation.

According to the "impurity induced twinning" model, increased twin formation arises from individual modifier atoms adsorbed at the solid-liquid growth front of Si. They are thought to alter the stacking sequence into a twin configuration [3]. However, the EDX mapping of Sr in Fig. 3 indicates that Sr found at the twins has not segregated atomically. It has been suggested [3] that a geometrical size factor (atomic radius of impurity element) could be the first and principal requirement for the promotion of "impurity induced twinning" [3]. An ideal geometrical size factor – i.e. ratio of radii of impurity atom and Si atom – of 1.646 was calculated [3]. However, neither Sr (ratio = 1.84) nor Na (ratio = 1.58) that are among the best modifiers satisfy this condition. On the other hand, Ca with a near-ideal ratio of 1.68 exhibits less modifying efficiency [3,34]. Therefore, from our results we conclude that it is not the geometrical size factor that plays a major role but rather the chemistry of the co-segregations. The fact that Sr was found to segregate together with Al and with the main component Si on the nm scale is indicative that the combination of all these elements promotes the generation of new twins and not individual modifier atoms as postulated earlier [3]. The promotion of twins by Sr–Al–Si co-segregation of type I is schematically explained in a modified illustration of the "impurity induced twinning" model, see Fig. 6(a). Such a rod-like Sr–Al–Si co-segregation (appearing as spots in the TEM) is adsorbed at {111} growth steps of the eutectic Si phase at the solid-liquid growth front and causes changes in the stacking sequence of {111} planes into A-B twin configurations for multiple twinning and, thus, is responsible for the increased density of twins in the eutectic Si phase. The chemical compositions of co-segregations of type I or type II derived from the proxigrams (Fig. 2(f) and 4(c)) correspond to about $SrAl_4Si_{33}$ or $SrAl_2Si_{88}$, respectively. Assuming the formation of intermetallic phases of stoichiometric compositions $SrAl_4Si_{33}$ or $SrAl_2Si_{88}$ at a temperature of 577°C (eutectic equilibrium temperature for Al–Si) the calculated Gibbs free energies correspond to −9 kJ/mol or −4 kJ/mol, respectively. In a recent study, twelve types of $Sr_{1-x-y}Al_xSi_y$ intermetallic phases were calculated applying density functional theory [35]. Sr–Al–Si intermetallic phases with compositions close to those of the present work were not mentioned, but according to the Gibbs free energy their formation is possible.

Statistical density spectrum analysis [36] was applied to the investigated volume. It reveals that Sr atoms are not homogeneously distributed in the eutectic Si phase and that only 20% of all Sr atoms in the volume shown in Fig. 2(a) correspond to rod-like co-segregations of type I. The Sr density in these segregated regions is 20–50 times

above that in segregation-free regions. Such segregations are not homogeneously distributed in the entire investigated volume, see Fig. 2(a), which is consistent with TEM observations of the distribution of twins. Some regions of the eutectic Si phase exhibit a high density of twins, others only very few, as TEM reveals (not shown). Due to the present results, the inhomogenous distribution of twins (as observed by TEM) and Sr–Al–Si co-segregations (as observed by APT) can be explained by a local Sr-enriched liquid at the eutectic growth front leading to a periodic interaction with the growth steps of Si and a subsequent incorporation of Sr–Al–Si intermetallic phases into the Si crystal. The importance of {111} twinning for the growth of the eutectic Si phase has been outlined in the introduction. Extensive studies have been carried out to explain modified eutectic growth by multiple twinning [3,21,34]. However, in a recent study it has been found that there is no significant difference in twin density between alloys displaying fine fibrous modification (by Ba and Ca) or refined plate-like Si morphology (by Y and Yb) [37]. This casts doubts on such explanations and suggests that the twin density is generally too low to explain modification alone. Considering our findings and those of Refs. 37 and 38, one can conclude that Sr does lead to higher twin density but that this does only indirectly contribute to eutectic modification due to a more uniformly oriented growth of eutectic Si phase in crystallographic directions other than <112>.

The extended rod-like Sr–Al–Si co-segregations (type II) shown in Fig's. 4 and 5(a) are initiated at the eutectic Al/Si interface and were found at internal boundaries of the eutectic Si phase, see Fig. 5(d) and 5(e). Therefore, we suggest that this type II co-segregation plays a different role than type I. In accordance to the repeatedly proposed mechanism of restricted growth [5,10,39,40] we suggest that Sr–Al–Si co-segregations of type II are adsorbed at the solid-liquid growth front of Si at the re-entrant edges and in this way prevent a further attachment of Si atoms to the growing crystal (by the TPRE mechanism) as schematically illustrated in Fig. 6(b). Due to the restriction of the TPRE growth mechanism the Si crystal is forced to change its growth to energetically favoured directions. The loss of the TPRE growth advantage causes eutectic Al phase to grow ahead of the eutectic Si phase and thus induces the change in the morphology of eutectic Si phase. The assumption of Al overgrowing Si is in accordance with previously observed overmodification bands of pure Al [38,40,41] when an excess (i.e. >100 ppm) of the modifier Na is added. The microscopically visible structure of overmodification bands has been explained by a

periodic build-up, i.e. local segregation, of a Na-enriched layer and subsequent formation of an Al–Si–Na intermetallic phase in wave-like patterns [41,42]. With the present results for Sr-modified Al–10 wt.% Si alloy, and with respect to other modifiers such as Ca, Ba and Eu, a similar periodic build-up and the formation of nanoscale X–Al–Si (X = Ca,Ba,Eu) intermetallic phases in the eutectic Si phase may play the key role in modifying Al–Si alloys.

Whereas type I co-segregations mainly contribute to the formation of new twins in the eutectic Si phase during growth, see Fig. 6(a), it is for type II that contributes to the branching of the Si fibres and not the non-co-zonal twinning as it has been assumed previously [21].

5. CONCLUSIONS

Combined APT and TEM investigations of the eutectic Si phase in Sr-modified (200 ppm) Al–10 wt.%Si–0.1 wt.%Fe alloy demonstrated that type II Sr–Al–Si co-segregations inhibit and restrict growth of the eutectic Si phase and thus induce a morphological change to a highly branched arrangement of eutectic Si phase. Type I Sr–Al–Si co-segregations change the stacking fault of {111} growth steps of the eutectic Si phase and thus induce twinning. We could show where exactly the Sr atoms are located in the eutectic Si phase and relate the Sr–Al–Si co-segregations found with previously postulated mechanisms of chemical modification of eutectic Si phase. The Sr–Al–Si intermetallic phases identified in the present study are worth being further investigated with respect to their chemical interaction with atomic scale defects (e.g. TPRE) of the eutectic Si phase, e.g. by density functional theory calculations showing that the Sr–Al–Si co-segregations do in fact change the stacking fault energy. Analyzing the eutectic microstructure of Al–X–Y (X = Si, Ge Y = Na, Ca, Ba, Eu) systems on the nm-scale could help to confirm the role of nanoscale Sr–Al–Si intermetallic phases both enabling impurity induced twinning and restricting TPRE growth of eutectic Si phase. Moreover, the results in the present study may have the potential to expand the knowledge of controlling Si defects in other applications, e.g. in the semiconductor industry.

ACKNOWLEDGEMENTS

The authors gratefully thank the DFG for financial support via grants Wa 1378/18, Wa 1378/20 and Ba 1170/19. The TEM study was partly carried out on the "Nanotechnology Network Japan" program sponsored by MEXT of the Japanese Government.

References

[1] Sigworth GK, Int J Metalcast 2008;2:19.

[2] Mondolfo LF, J Aust Inst Met 1965;10:169.

[3] Lu SZ and Hellawell A, Metall Mater Trans A 1987;18:1721.

[4] Pacz A, Alloy. U.S. Patent No. 1387900;1921.

[5] Day MG and Hellawell A, Proc Roy Soc 1968;*A* 305:473.

[6] Schulz E, Z Metallkde 1949;39:123.

[7] Thall BM and Chalmers B, J Inst Met 1950;77:79.

[8] Tsumara Y, Nippon Kinzoku Gakkai-Si 1957;21:69.

[9] Davies VdL and West J, J Inst Met 1963–64;92:208.

[10] Kobayashi KF and Hogan LM, J Mater Sci 1985;20:1961.

[11] Flood SC, Hunt JD. Metal Science 1981;15:287.

[12] Dahle AK, Nogita K, Zindel JW, McDonald SD, Hogan LM. Metall Mater Trans A 2001;32:949.

[13] Nogita K, McDonald SD, Tsujimoto K, Yasuda K, Dahle AK. J Electron Microsc 2004;53:361.

[14] Shankar S, Riddle YW, Makhlouf MM. Acta Mater 2004;52:4447.

[15] Campbell J, Tiryakioglu M. Mater Sci Technol 2010;26:262.

[16] Makhlouf M, Guthy H. J Light Met 2001;1:199.

[17] Gruzleski JE. AFS Trans 1992;100:673.

[18] Hegde S, Prabhu KN. J Mater Sci 2008;43:3009.

[19] Hamilton DR and Seidensticker RG, J Appl Phys 1960;31:1165.

[20] Shamsuzzoha M and Hogan LM, J Cryst Growth 1986;76:429.

[21] Shamsuzzoha M and Hogan LM, Phil Mag A 1986;54:459.

[22] Clapham L and Smith RW, J Cryst Growth 1988;92:263.

[23] Nogita K, Yasuda H, Yoshida K, Uesugi K, Takeuchi A, Suzuki Y and Dahle AK, Scripta Mater 2006;55:787.

[24] Kellogg GL and Tsong TT, J Appl Phys 1980;51:1184.

[25] Thompson K, Flaitz PL, Ronsheim P, Larson DJ, and Kelly TF, Science 2007;317:1370.

[26] Gault B, Vurpillot F, Vella A, Gilbert M, Menand A, Blavette D, and Deconihout B, Rev Sci Instrum 2006;77:043705

[27] Larson DJ, Foord DT, Petford-Long AK, Liew H, Blamire MG, Cerezo A, and Smith GDW, Ultramicroscopy 1999;79:287

[28] Thompson K, Lawrence D, Larson DJ, Olson JD, Kelly TF and Gorman B, Ultramicroscopy 2007;107:131

[29] Choi PP, Al-Kassab T, Kwon YS, Kim JS and Kirchheim R, Microsc Microanal 2007;13:347

[30] Schlesiger R, Oberdorfer C, Würz R, Greiwe G, Stender P, Artmeier M, Pelka P, Spaleck F and Schmitz G, Rev Sci Instrum 2010;1:043703

[31] Lasagni F, Lasagni A, Marks E, Holzapfel C, Mücklich F and Degischer HP, Acta Mater 2007;5:3875.

[32] Timpel M, Wanderka N, Murty BS and Banhart J, Acta Mater 2010;58:6600.

[33] Hellman OC, Vandenbroucke JA, Rüsing J, Isheim D and Seidman DN, Microsc. Microanal. 2000;6:437.

[34] Nogita K, Drennan J and Dahle AK, Mater Trans 2003;44:625.

[35] Garay-Tapia AM, Romero AH, Trapaga G and Arróyave R, Intermetallics 2012;21:31

[36] Wanderka N, Lazarev N, Chang CST and Banhart J, Ultramicroscopy 2011;111:701.

[37] Nogita K, Yasuda H, Yoshiya M, McDonald SD, Uesugi K, Takeuchi A and Suzuki Y, J Alloys & Comp 2010;489:415.

[38] Fredriksson H, Hillert M and Lange N, J Inst Met 1973;101:285.

[39] Atasoy ÖA, Z Metallkde 1987;78:177.

[40] Liu Q, Li Q and Liu Q, Acta Metall Mater 1991;39:2497.

[41] Crosley PB and Mondolfo LF, AFS Trans 1966;74:53.

[42] Kobayashi K, Shingu PH and Ryohei O, T Jpn I Met 1980;21:417.

Table 1

Chemical composition of unmodified and Sr-modified Al-10Si casting alloy measured by optical emission spectrometry. The amount of main elements Al, Si and Fe are given in wt%, whereas the additional trace elements are in ppm.

Alloy	Al	Si	Fe	Cu	Mn	Mg	Cr	Ti	Ni	Ga	V	P	**Sr**
	(wt.%)			(ppm)									
Unmodified	89.1	10.1	0.1	10	20	10	11	61	38	41	102	3	**<1**
Sr-modified	89.1	10.0	0.1	10	20	10	11	60	38	42	102	4	**200**

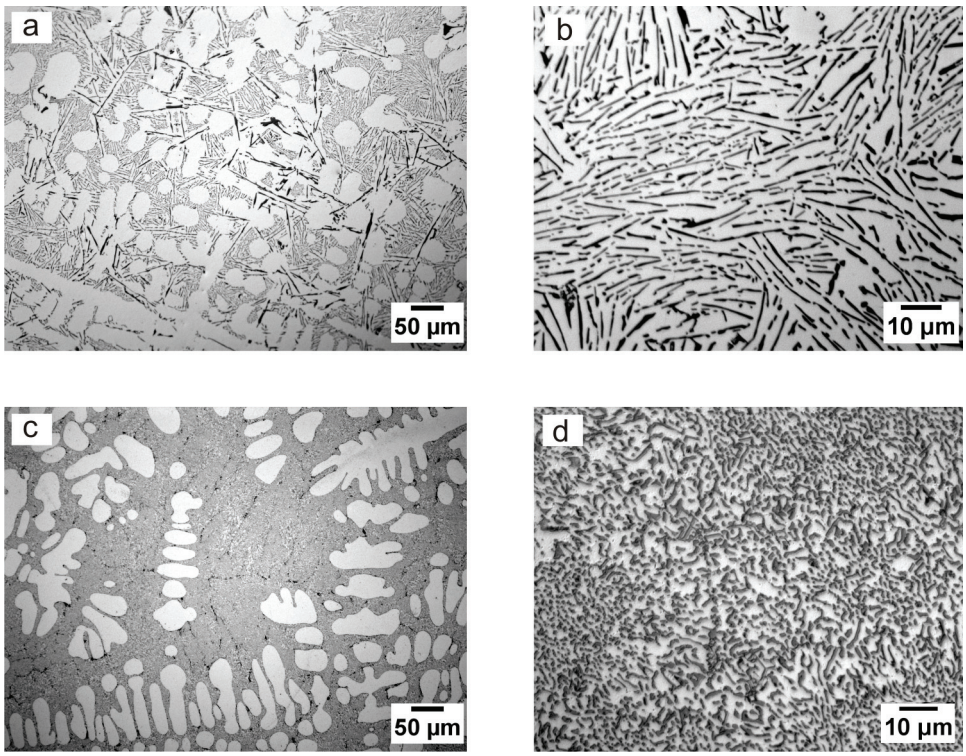

Fig. 1. Optical micrographs of Al–10 wt.% Si–0.1 wt.% Fe alloy showing a eutectic microstructure: (a and b) unmodified alloy, (c and d) alloy modified by 200 ppm Sr.

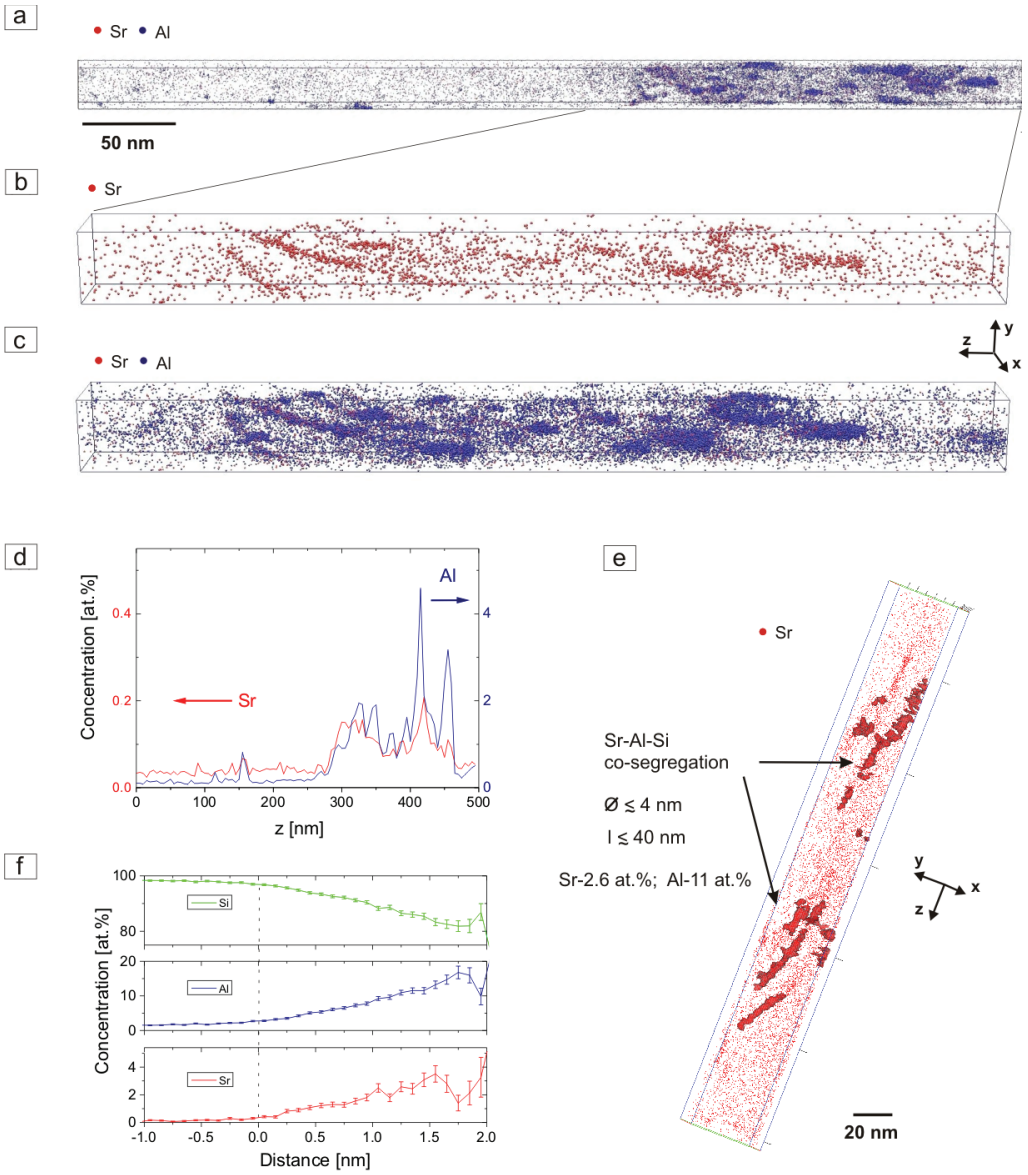

Fig. 2. Atom probe tomography of eutectic Si phase in Al– 10 wt.% Si– 0.1 wt.%Fe alloy modified by 200 ppm Sr: (a) 3-D reconstruction of Sr (red dots) and Al (blue dots) atom positions in an analysed volume of 20 × 20 × 500 nm^3. Si atoms are omitted for clarity. (b) 3-D Sr (red dots) atom distributions in a part of analysed volume in (a). (c) 3-D Sr (red dots) and Al (blue dots) atom distributions within the subvolume shown in (b). (d) Concentration depth profiles of Sr and Al along the experimental axis of the entire volume in (a). (e) 3-D reconstruction of Sr atoms showing the iso-concentration surface representing 0.6 at.% Sr that is used to define the Si/Sr–Al co-segregation interface. (f) Proxigram showing Sr, Al and Si concentrations as a function of distance to the Si/Sr–Al co-segregation interface given in (e).

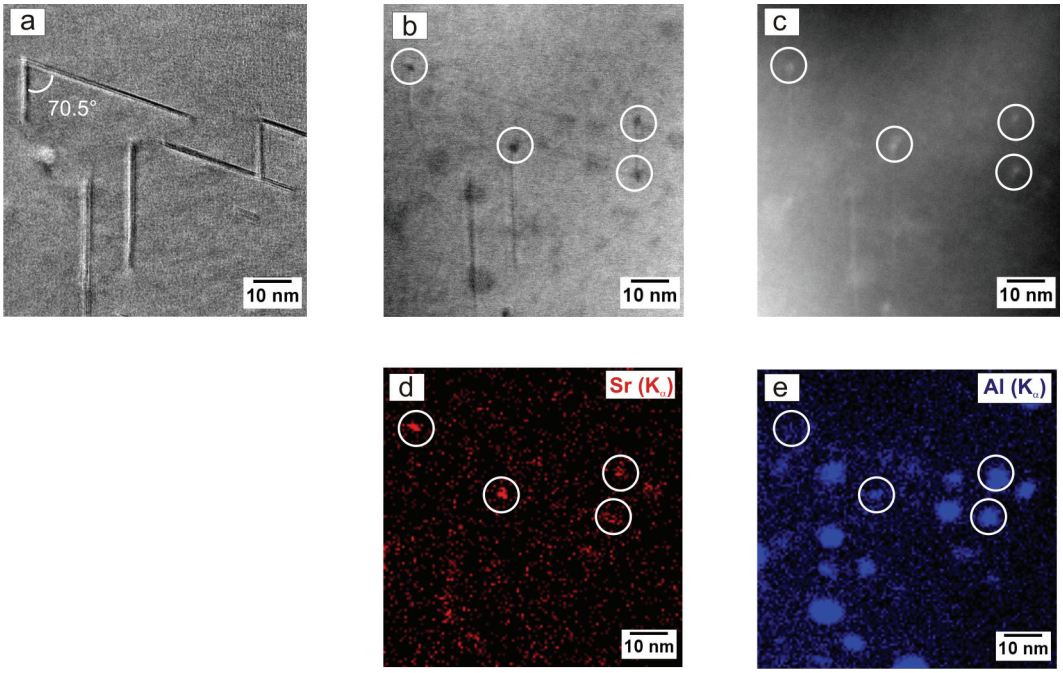

Fig. 3. Microstructure of one and the same area within a eutectic Si phase in Al–10 wt.% Si–0.1 wt.% Fe alloy modified by 200 ppm Sr obtained using: (a) HRTEM. (b) BF STEM. (c) HAADF STEM. (d) EDX mapping of Sr. (e), EDX mapping of Al. Circles mark co-segregation of Sr and Al.

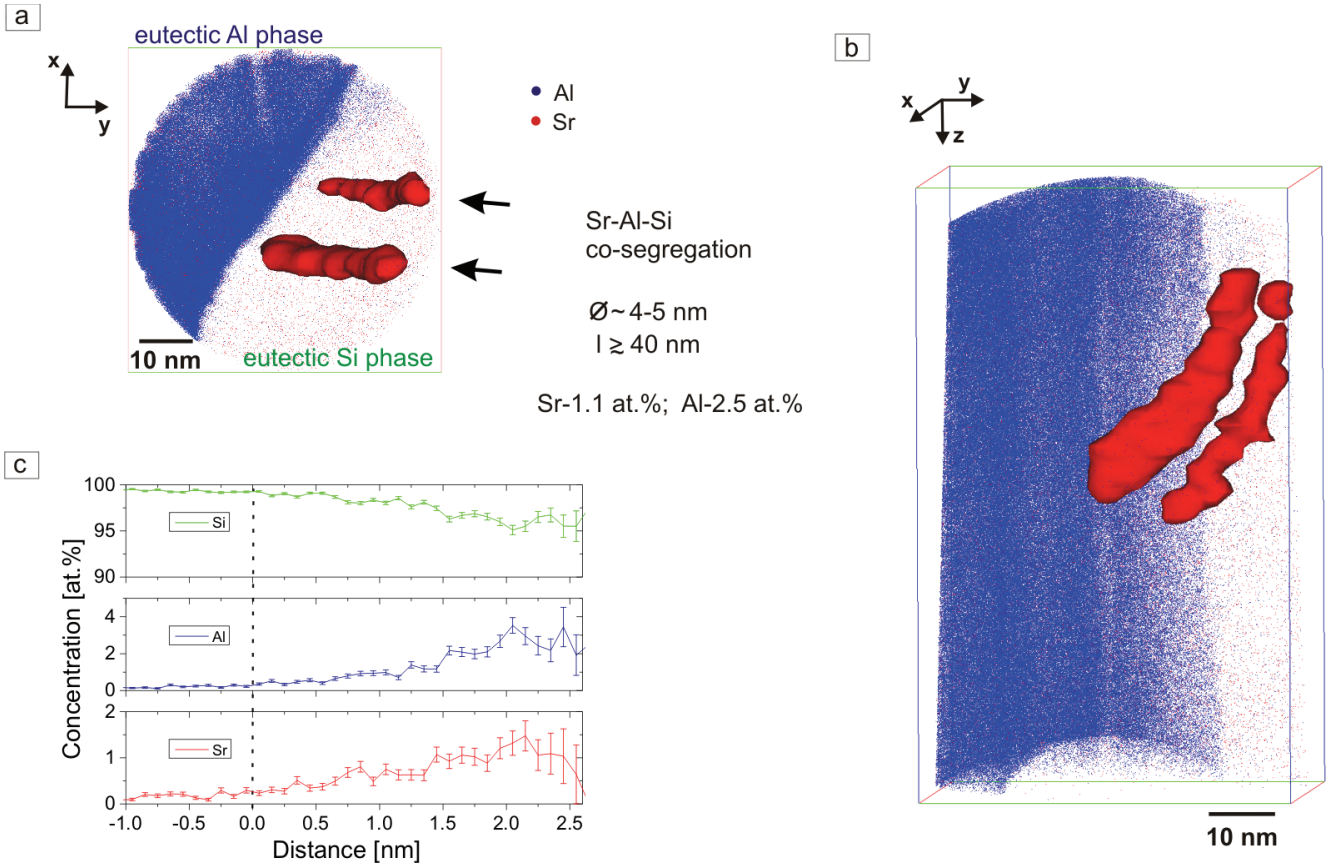

Fig. 4. Atom probe tomography of eutectic Al/Si interface in Al–10 wt.% Si–0.1 wt.% Fe alloy modified by 200 ppm Sr. 3-D reconstruction of Sr (red dots) and Al (blue dots) atom positions in analysed volume of 58 × 56 × 93 nm^3, top view in (a) and front view in (b). Si atoms are omitted for clarity. Iso-density surface in (a), and (b), representing 0.17 Sr atoms/nm^3 in both co-segregations. (c) Proxigram showing Sr, Al and Si concentrations as a function of distance to the Si/Sr–Al–Si co-segregation interface given in (a) and (b).

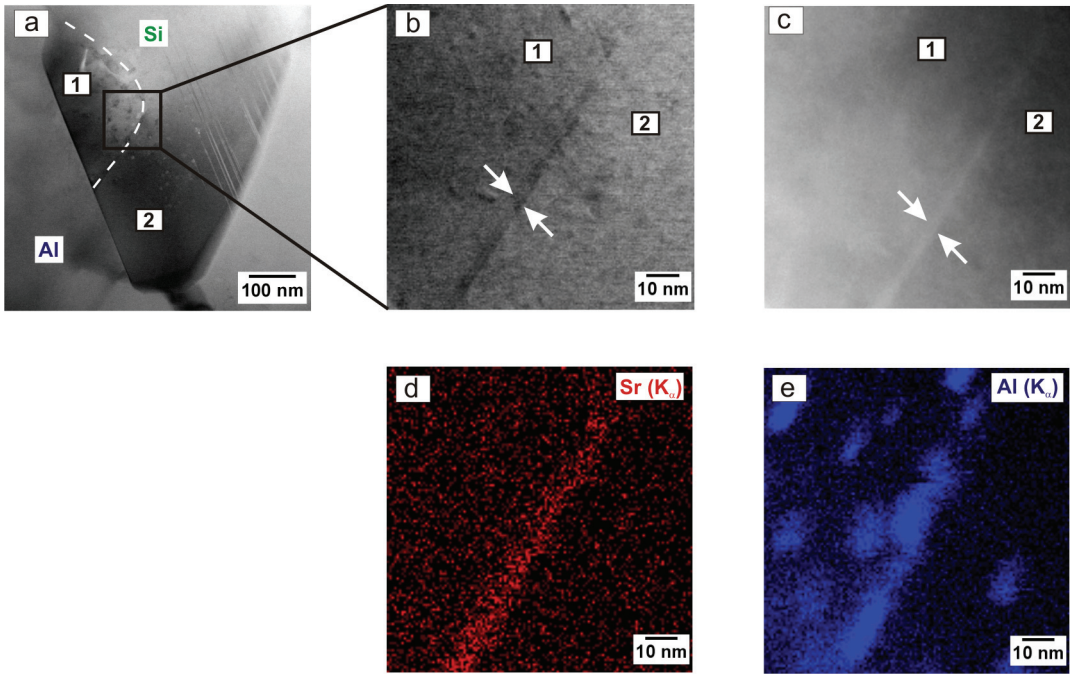

Fig. 5. Microstructure showing a eutectic Al/Si interface of Al–10 wt.% Si–0.1wt. % Fe alloy modified by 200 ppm Sr: (a) BF STEM image. An internal boundary of the eutectic Si phase along a {111} plane is visible. Both Si fibre segments are oriented close to the [011] zone axis. An enlarged view of the area marked by the rectangle in (a) is imaged using: (b) BF STEM, (c) HAADF STEM, (d) and (e) EDX mapping of Sr and Al, respectively. The internal boundary of the eutectic Si phase is marked by arrows in (b) and (c).

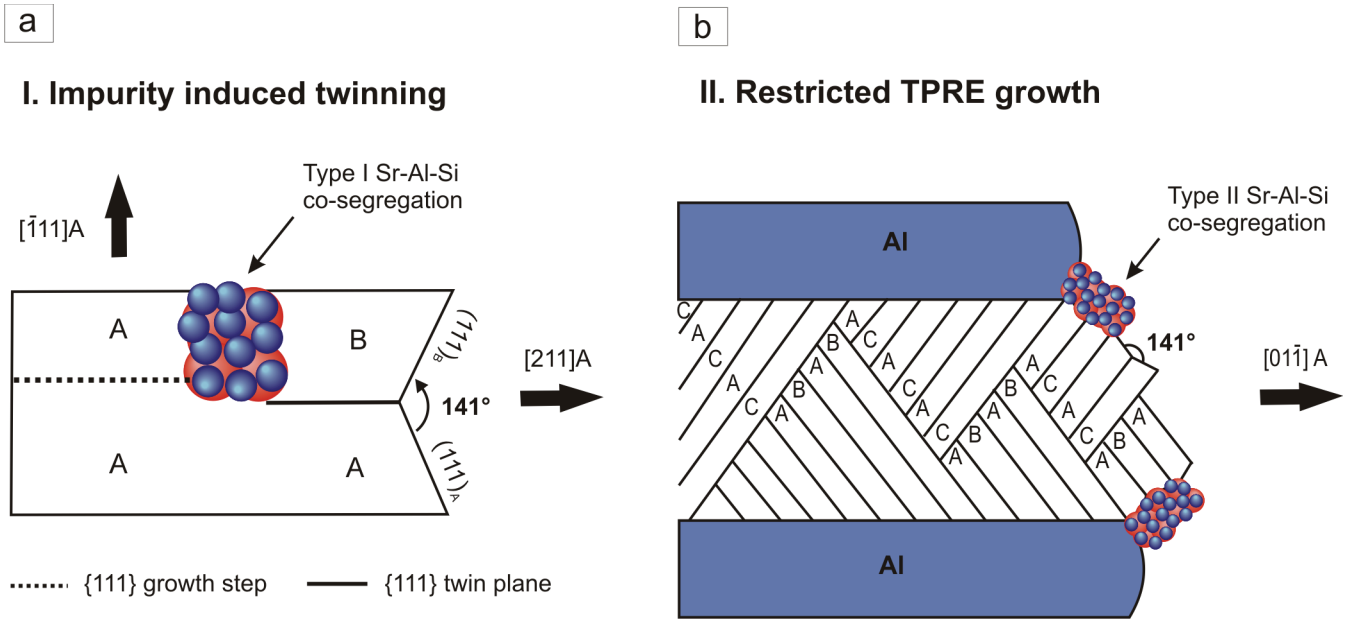

Fig. 6. Schematic representation of (011) plane projection of eutectic Si phase: (a) type I Sr–Al–Si co-segregation which promotes twinning by changing the stacking sequence. (b) locations of type II Sr–Al–Si co-segregations within the eutectic Si phase at the re-entrant edges or growing surfaces.